

ACCELERATOR STRUCTURE DEVELOPMENT FOR ROOM-TEMPERATURE LINACS

S.O. Schriber

Atomic Energy of Canada Limited
Chalk River Nuclear Laboratories
Chalk River, Ontario K0J 1J0

Summary

Developments in room-temperature cavities for standing-wave structures are reviewed. These include cavity geometries, assembly techniques and material choices. This review includes structures for storage rings, microtrons and linear accelerators. Design constraints for 100% duty cycle and high-gradient low duty cycle structures are discussed emphasizing high current operation and areas for new development.

Introduction

Developments in room-temperature structures have been in three areas - improving rf efficiency, simplifying fabrication and improving operating characteristics. These areas are important for high beam-loaded, high duty-cycle accelerators and pulsed high-gradient accelerators, mainly because of economic, cooling and space requirements.

This paper discusses features of room-temperature standing-wave structures emphasizing characteristics of coupled-cavities operated in the $\pi/2$ mode. Considerations for peak field stress are given because of their relevance to high-gradient structures and the newly developed radiofrequency quadrupole structure.

Field Stress

A criterion for determining regions of possible sparking and no sparking was developed in the 1950's by Kilpatrick¹. His gap-independent-effect formula yields what is called in this paper the Kilpatrick field limit, KL, for any frequency:

$$f = 1.64 E^2 e^{-8.5/E}$$

where f is the frequency in MHz below which sparking is possible for peak electric field E in MV/m.

Pulsed room-temperature structures have operated to at least twice KL for a large range of frequencies and rf structures including the radiofrequency quadrupole linac², drift tube linac³ and coupled-cavity linac⁴. Generally, 100% duty cycle (cw) structures are not operated at high field stress because of severe cooling problems associated with high rf losses. Proton acceleration in the 12 MHz cw MTA⁵ showed that a drift tube linac could operate at KL. With the first drift tube removed, the structure operated to 1.5 KL. Based on this information and in the absence of electron loading between gaps, a cw accelerator designed to 1.5 KL should perform without excessive field breakdown. Operation at 1.75 KL might be satisfactory.

Further experiments on high fields will either demonstrate ease of operation or reveal problems associated with radiation fields. Experiments on heavily beam-loaded structures will provide information relevant to high field stress operation as well as pertinent data related to reactive beam loading and higher order mode losses.

Low Beta Structures

The most recent development in low beta structures is the radiofrequency quadrupole (RFQ) system,

originally conceived by Kapchinskii and Teplyakov⁶ and developed extensively in the four-vane geometry at LASL^{2,7}. Advantages of an RFQ are acceptance of a low energy beam, ~ 50 keV/amu, and the bunching and acceleration of this beam to moderate energy, ~ 2 MeV/amu, with greater than 90% beam transmission. Figure 1 shows a cross-sectional octant of the geometry as viewed along the structure axis. Extensive calculations, with a modified SUPERFISH code that normalizes RFQ geometries to 100 kV on the vertical vane tip, have shown that the four-vane rf loss per unit length, P/l, in W/m is given by:

$$P/l \approx 1.47 \times 10^{-18} V^2 f^{1.5} / R_H^{0.3}$$

where V is the vane tip voltage in volts, f is the rf frequency in Hz and R_H is the average aperture radius in cm (see Fig. 1).

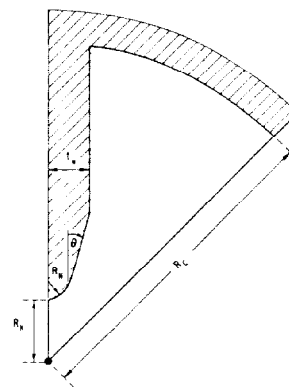


Fig. 1 Cross-sectional octant of four vane RFQ geometry.

Figure 2 gives rf loss and outer cylinder radius as a function of the average aperture radius for 270 MHz RFQ geometries with vane voltage normalized to 100 kV.

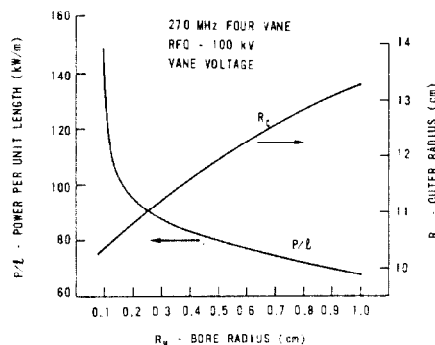


Fig. 2 270 MHz RFQ rf power loss per unit length, P/l, and outer radius, R_c , as a function of bore radius, R_b .

Rf losses increase with increasing volts and frequency for the same beam aperture. Since focusing

strength is proportional to V/R_H^2 (see reference 7), rf losses increase as $R_H^{3.7}$ for the same focusing strength in larger aperture structures. For example, RFQ geometries being studied at CRNL for 300 mA proton acceleration at 108 MHz require average aperture radii greater than 2 cm and rf powers in excess of 500 kW for the 4 m of rf structure losses. Beam dynamics constraints require as high a vane voltage as possible, with fields greater than 1.5 KL.

An rf loss study has shown that the angle, θ , from the vane tip to the flat portion of the vane and the vane half thickness, t_w , should be small, consistent with machining, cooling and assembly requirements - the former being $< 30^\circ$. RF loss increases by $\sim 2\%$ per degree increase in θ if this angle were continued back to the outer radius. A 50% increase in t_w increases loss by $\sim 20\%$. A maximum decrease of 10% in loss can be achieved by curving the corner between the vane and the outer cylinder. Power loss on the vane section with thickness t_w increases by approximately the square root of the distance from the structure axis - loss on the first 10% of the vane flat is one half of that on the last 10% closest to the outer radius. For cw operation good cooling and mechanical support are necessary to maintain dimensional tolerances - requirements important for the drift-tube linac structure as well.

An efficiency improvement for drift-tube linac structures can be realized by large face angles on the drift tubes - improvements⁸ of better than 15% are possible with angles larger than 15° .

Coupled Cavity Linacs

Cross-sections of three room-temperature standing-wave structures for high-beta acceleration in the $\pi/2$ mode are shown schematically in Fig. 3 - the side-coupled, the disk-and-washer and the on-axis coupled geometries. Diameter is largest for the disk-and-washer structure and smallest for the on-axis coupled structure. The on-axis coupled structure is easiest to fabricate and assemble because components are similar and coaxial. Of the three geometries, it should operate best in a stressful environment because of its overall compactness. Rf efficiencies of side-coupled and on-axis coupled structures are similar with losses in side-couplers balanced by the effectively thicker web in the on-axis geometry. The disk-and-washer structure offers many advantages^{9,10} because of a high coupling constant and a more efficient geometry with more stored energy in the structure volume. This latter feature is an asset for highly beam-loaded systems.

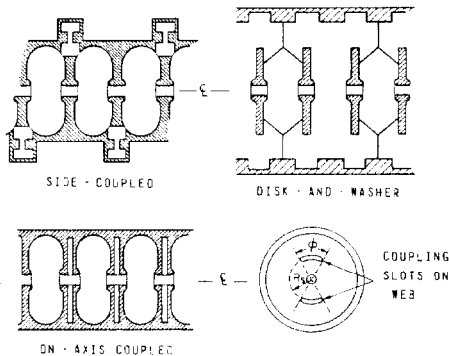


Fig. 3 Cross-sections of three room-temperature standing-wave structures with location of coupling slots shown for the on-axis coupled geometry.

Optimization of cavity profile in most instances is related to determining geometrical parameters that yield the highest rf efficiency. Figure 4 shows a quarter cross-section of the disk-and-washer cavity geometry and the shaped cavity geometry used in side-coupled and on-axis coupled structures. The angle, θ , of the drift-tube nose should be $\leq 30^\circ$ and the web thickness, t_w , should be small, consistent with mechanical and cooling constraints. The most important parameter to maximize rf efficiency is the g/L ratio. Table 1 gives optimum g/L ratios for $\beta=0.4$ to 1.0 cavities with bore-hole radii of 0.55 to 4.4 cm at 1350 MHz - the ratios apply to both cavity geometries. A $\beta=1.0$ cavity with large bore radius and optimum g/L ratio has very little drift-tube nose.

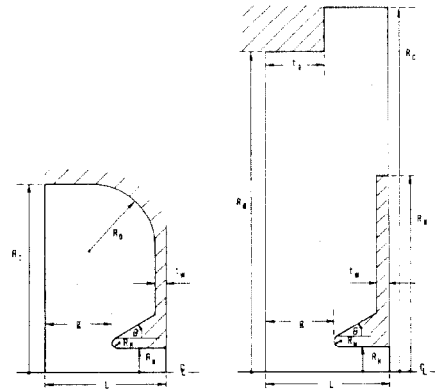


Fig. 4 Quarter cross-sections of the shaped cavity and the disk-and-washer cavity showing geometrical parameters.

Table 1

Optimum g/L Ratios for Coupled Cavity Structures

Bore Hole Radius at 1350 MHz cm (R_H/λ)	$\beta=0.4$	$\beta=0.6$	$\beta=0.8$	$\beta=1.0$
0.55 (0.0248)	0.22	0.33	0.44	0.55
1.1 (0.0495)	0.31	0.42	0.52	0.62
2.2 (0.0991)	0.41	0.53	0.65	0.72
4.4 (0.1981)	0.47	0.59	0.74	0.81

Accelerating gradients of 40 MeV/m at 3000 MHz should be attainable, with 1.6 KL field stress, using structure geometries that have no drift-tube nose and 0.5 cm bore radius. Theoretical efficiencies for the shaped cavity and disk-and-washer geometries are 80 and 104 MΩ/m respectively - values that are 80% of optimum geometry values.

An outer radius of curvature, R_o , for the inside corner of the shaped cavity geometry can improve rf efficiency up to 10%, at the expense of a larger cylinder radius, R_c . The necessity for a finite R_o in the final geometry is determined by machining capabilities and other constraints. R_c is chosen to give the desired frequency of the $\pi/2$ accelerating mode (denoted $\pi/2A$). The $\pi/2$ coupling mode frequency ($\pi/2C$) is made equal to the $\pi/2A$ frequency by adjusting the side-coupler boss separation or the radius of the on-axis coupling cavity.

The disk-and-washer geometry has an extra degree of freedom because R_c can be picked to fit mechanical

constraints, to yield high rf efficiency and to be equal for all betas. R_c/λ should not exceed 0.81 to minimize mode overlapping in the region of the $\pi/2$ mode and to retain high group velocity characteristics. Radii of the washer, R_w , and the disk, R_D , are specified to make frequencies of the $\pi/2A$ and $\pi/2C$ equal. The disk thickness, t_D , is optimized as well.

Structures are fabricated from OFHC copper for efficiency reasons and to enable hydrogen brazing of component pieces. In some instances copper-clad steel would be the preferred material for reasons of strength, cost and minimizing certain geometrical parameters. Elaborate cooling methods^{11,12} need to be employed in cw applications because every 5° rise in average temperature results in a 1% loss in rf efficiency.

Side-Coupled Structure

Coupling constants of 5% are easily attained with this geometry. $\pi/2A$ and $\pi/2C$ tuning is accomplished by separately tuning the accelerating half cavity and the side-coupler cavity to individual frequencies that yield equal mode frequencies in an assembled system. One assembly method involves brazing segments consisting of two adjacent half cavities followed by a braze of all coupling cavities to the brazed segment assembly. Another fabrication method involves brazing side-couplers to their respective segments followed by a braze of all segment-coupler assemblies. Preferred brazing alloys are discussed in reference 13. Many side-coupled structures are being operated and the reader is referred to extensive literature for more details.

On-Axis Coupled Structures

As above, the half accelerating cavity and the on-axis coupling cavity are tuned separately to produce the desired frequency when assembled. Assembly consists of brazing segments consisting of half accelerating cavity and half coupling cavity.

Figure 5 shows results of measurements for a 3000 MHz on-axis coupled structure with a 2.06 cm coupling slot radius, R_s . The intercavity coupling constant, k , and the coupling cavity radius R_{cc} , required for tuned conditions are shown as functions of t_w for different coupling cavity lengths. Since structure stability is proportional to k^2 , coupling cavity length and t_w should be small, consistent with cooling and mechanical constraints.

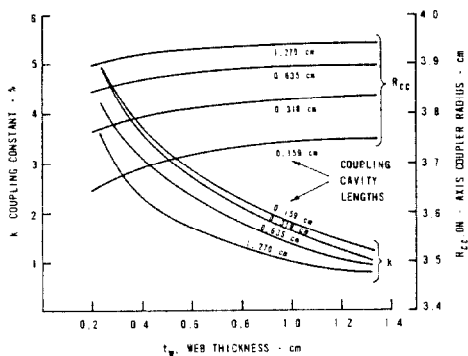


Fig. 5 Intercavity coupling, k , and coupler radius, R_{cc} , as a function of web thickness, t_w , for different coupler lengths.

Measurements shown in Fig. 6 demonstrate that coupling constants up to 23% can be obtained by increasing the angle, ϕ , of the coupling slot. Higher coupling constants would be difficult to achieve with this geometry because the value of R_{cc} has decreased to that of R_s . The coupling slot width need not exceed 0.06λ because k does not increase appreciably for larger widths. References 4, 9 and 11 describe operating on-axis coupled structures.

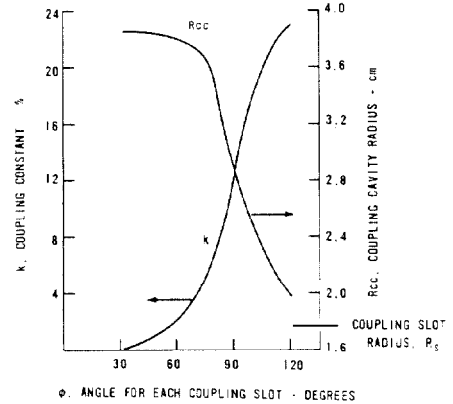


Fig. 6 Intercavity coupling, k , and coupler radius, R_{cc} , as a function of slot angle, ϕ .

Disk-and-Washer Structure

Characteristics of optimized 1320 MHz geometries are given in Table 2 for betas from 0.4 to 1.0. Two numbers in the column marked "peak on-axis" represent the trough and peak for on-axis field distributions that have a double peak nature. The structure can be terminated in several ways⁹ - one being a half-cavity configuration, the power for which is given under "end wall", and another being a shaped termination as shown in Fig. 7, the power for which is given under "shaped termination". This structure offers many attractive features but has encountered some difficulties associated with washer supports.

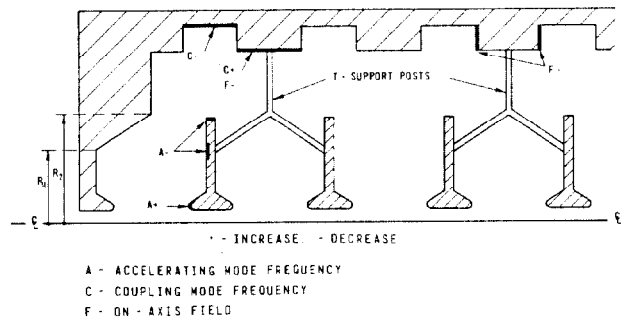


Fig. 7 Schematic of 1320 MHz, $\beta=1.0$ disk-and-washer structure showing ideal location for washer supports and end termination. Regions for tuning the accelerating and coupling modes, and for altering on-axis fields are given with an indication of increase or decrease.

Disk-and-washer tuning can be accomplished using assemblies consisting of two half cavities and one full cavity formed when two washers are joined by common T supports to an outer cylinder and disk, or with larger assemblies. Locations for removing material during tuning to increase or decrease the accelerating, A, and coupling, C, mode frequencies are shown in Fig. 7.

Table 2

Parameters for Disk-and-Washer Linac Structure at 1320 MHz
 Half Cavity Values Normalized to 1 MV/m Average On Axis Fields
 $t_w=0.4$ cm, $R_N=0.25$ cm, $R_H=1.111$ cm, $R_C=16.6$ cm, $\theta=30^\circ$

Beta	L cm	q/L	r _D cm	R _C cm	R _W cm	ZT ² MG/m	Q	Z/D	E _{max} kV/m	Peak On Axis MV/m	Stored Energy mJ	Cavity Power W	End Wall W	Shaped Term W	Shape Location		% Power on Cavity			T	
															R ₁ cm	R ₂ cm	Cyl	Disk	Washer		
0.4	2.271	0.336	0.36	11.71	11.27	32.17	19087	2.321	5.37	2.12	-	1.182	512.7	470.9	612.7	7.50	7.50	0.004	1.52	98.48	0.852
0.5	2.839	0.353	0.61	12.05	10.95	45.27	24414	2.499	5.03	2.12	-	1.373	465.4	420.2	609.1	7.48	7.52	0.013	2.06	97.93	0.361
0.6	3.407	0.415	0.92	12.45	10.63	56.76	29815	2.567	4.78	1.99	-	1.602	445.1	401.7	629.8	7.42	7.59	0.04	2.96	97.0	0.361
0.7	3.975	0.462	1.30	12.87	10.31	66.62	35430	2.574	4.71	1.82	1.83	1.865	435.9	402.2	660.5	7.35	7.73	0.10	4.52	95.38	0.855
0.8	4.542	0.504	1.72	13.32	9.94	75.18	41746	2.527	4.62	1.66	1.73	2.170	420.6	421.2	699.4	7.14	8.01	0.23	7.02	92.75	0.844
0.9	5.110	0.545	2.18	13.86	9.52	82.56	49780	2.406	4.51	1.51	1.67	2.563	426.6	469.5	758.6	6.75	8.63	0.51	11.42	88.06	0.830
1.0	5.678	0.582	2.71	14.54	8.93	88.08	61212	2.165	4.45	1.40	1.62	3.145	428.5	578.7	823.2	6.16	9.24	1.20	20.15	78.66	0.815

Table 3 gives frequency sensitivities of the different geometric sections in MHz/cm at 1320 MHz for the accelerating mode and in brackets for the coupling mode. T-supports introduce a quadruperic nature to the dispersion curve.

Table 3

Parameter Variation in MHz/cm at 1320 MHz
 $R_C=16.6$ cm, $t_w=0.4$ cm, $R_H=1.1$ cm, $\theta=30^\circ$, $R_N=0.25$ cm
 Accelerating Mode (Coupling Mode)

Parameter	$\theta=0.4$	$\theta=0.6$	$\theta=0.8$	$\theta=1.0$
R _C	-2.2(-201.6)	3.9(-184.5)	3.7(-164.7)	3.8(-115.8)
R _D	3.7(230.1)	3.8(194.5)	1.6(161.8)	-6.2(104.2)
R _W	-90.0(- 43.2)	-100.4(- 18.1)	-92.0(- 4.5)	-76.3(0.9)
g	272.4(0)	161.1(0.01)	112.1(0.4)	72.6(5.1)
t _D	-15.9(- 91.3)	-10.4(- 17.0)	-7.8(15.5)	-5.3(21.0)
t _W	218.6(- 2.5)	135.3(- 0.9)	88.2(- 1.3)	44.9(1.3)
R _H	-60.0(0)	-50.3(- 0.01)	-45.6(- 0.3)	-28.3(- 2.9)

Figure 8 shows the 1320 MHz $\beta=0.9$ and 1.0 families of radii, R_1 and R_2 , for the shaped termination that yield correct frequency characteristics. Values of R_1 and R_2 are plotted versus the left (or terminating side) peak height to right peak height ratio of the double-peaked on-axis field distribution. Only one set for each beta, listed in Table 2, gives the desired on-axis field distribution that is symmetrical about the cavity centre. These radii also indicate ideal locations for the T-shaped washer support that should minimize asymmetries in adjacent cavity fields.

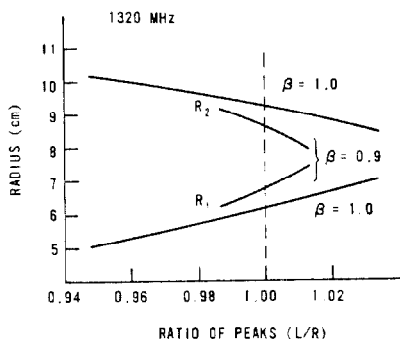


Fig. 8 Families of radii, R_1 and R_2 , for $\beta=0.9$ and 1.0 shaped terminations that yield tuned characteristics as a function of the left to right double peak ratio.

Experimentally it has been determined¹⁴ that on-axis fields in the cavities with T-shaped supports can be up to 25% high or low depending on cavity beta and

washer support location. Locations for removing material to decrease the on-axis field, F, of the cavity perturbed by this removal are indicated in Fig. 7. For a $\beta=1.0$, 2380 MHz geometry Fig. 9 gives the ratio of on-axis fields in the modified cavity to those in the unmodified cavity versus R_D and t_D variation. Adjusting t_D , the preferred means to compensate for field differences, results in small frequency shifts of 42 and -15 MHz/cm for the coupling and accelerating modes respectively. Studies have shown that R_C and R_D adjustments are not suitable

because the coupling mode frequency is changed significantly. Moving washers left or right from their ideal locations produces 10% field differences per mm movement at 2380 MHz without frequency shifts. This method introduces asymmetries that may not be suitable in terms of beam dynamics and assembly.

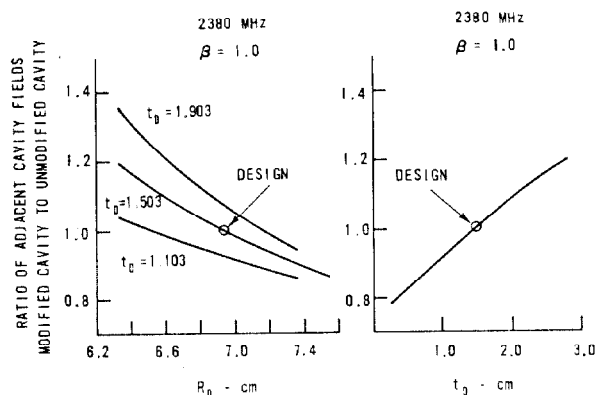


Fig. 9 Ratio of adjacent cavity fields versus disk radius, R_D , and disk thickness, t_D , at 2380 MHz.

The structure can be assembled by brazing disks and T-supported washer assemblies to a long outer cylinder or by brazing a chain of segments consisting of T-supported washers mounted to their respective disks and outer cylinder.

Figures 10 and 11 show rf efficiency or effective shunt impedance, ZT^2 , as a function of bore radius and beta using optimized geometries for a 17 cm outer cylinder radius structure at 1350 MHz. Similar curves are obtained for shaped cavity geometries. Choice of bore radius is very important. A 25% reduction in radius (from 1.1 cm) results in ZT^2 improvements of greater than 20% at low beta.

An interesting exercise in geometry selection is based on Fig. 12 where ZT^2 is given as a function of frequency for 0.55 cm bore radius. Assuming that the

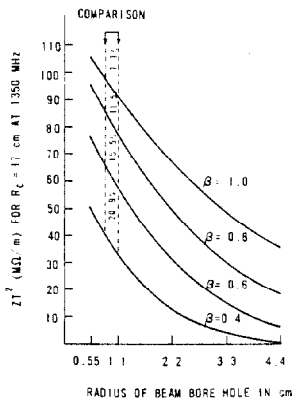


Fig. 10

Fig. 10 ZT^2 at 1350 MHz as a function of beam bore radius for betas from 0.4 to 1.0.

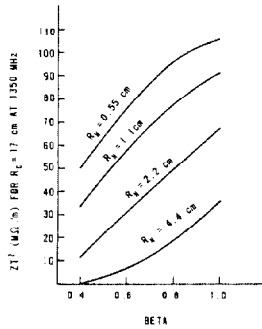


Fig. 11

Fig. 11 ZT^2 at 1350 MHz as a function of beta for beam bore radii from 0.55 cm to 4.4 cm.

choice of structure frequency has no constraints (consistent with available rf sources, power requirements, accelerating gradient, etc.), the only structure constraint is imposed by bore radius, R_H . Efficiency is

optimized not only by geometrical parameters but by selecting the operating frequency from Fig. 12. Two opposing variations are involved - ZT^2 increases with increasing frequency but decreases with increasing bore hole radius. For $\beta=1.0$ and $R_H=0.55$ cm, highest

efficiency is obtained at ~ 4400 MHz for the shaped cavity and the disk-and-washer geometries: 105 MQ/m and 138 MQ/m respectively. For $\beta=0.4$ and $R_H=0.55$ cm, highest efficiency of 52 MQ/m is obtained at ~ 1700 MHz.

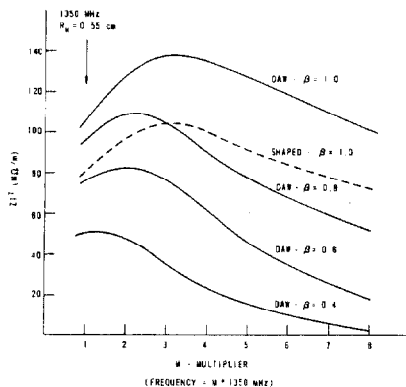


Fig. 12 ZT^2 as a function of frequency for different betas with 0.55 cm bore radius.

Figure 12 can be used for other bore hole radii. For example, a $0.55/\alpha$ cm bore radius would require the x-axis variable, M , to be multiplied by α and the y-axis ZT^2 scale to be multiplied by $\sqrt{\alpha}$. For $R_H=1.1$ cm and $\beta=1.0$, the maximum ZT^2 of 98 MQ/m would occur at ~ 2200 MHz. Similarly, the maximum ZT^2 of 69 MQ/m would occur at a frequency of ~ 1100 MHz for $R_H=2.2$ cm and $\beta=1.0$.

Discussion and Conclusion

Coupled cavity structures discussed above have been or will be operated in microtrons, linacs and

rings. Designs employing the disk-and-washer structure for microtrons and rings are being pursued at LASL. Reference 15 describes an on-axis coupled structure designed for use in an electron ring. Coupling slots are not required because ample coupling exists between cavities via the beam bore hole. Calculations with loop coupled RLC models have shown that this nine accelerating cavity structure operated in the $\pi/2$ mode with only one tuner will have slightly better field characteristics than a five cavity structure operated in the π mode and employing two tuners.

The disk-and-washer structure needs further development work on tuning, assembly methods, higher order mode characteristics and high-field operation. Many of its interesting properties should be fully exploited in the future. It is a good choice for high beam-loaded structures, either pulsed or cw, for two reasons: it has the highest stored energy per cavity and highest group velocity of the three structures described in this paper.

An on-axis coupled structure with high coupling could be used in systems requiring smaller outer dimensions or requiring simple and rugged assemblies. Inter-cavity coupling and ZT^2 of $\sim 1/3$ and $\sim 3/4$ respectively of that for the disk-and-washer, are penalties that may not be too restrictive in some instances.

References

1. W.D. Kilpatrick, "A Criterion for Vacuum Sparking Designed to Include both RF and DC", Radiation Laboratory Report UCRL-2321 (1953).
2. J.E. Stovall, K.R. Crandall and R.W. Hamm, "Performance Characteristics of a 425 MHz RFQ Linac", Conf. on Appl. of Accel. in Research and Industry, Denton, Texas, November 1980, to be published.
3. J.E. Stovall, "Initial Performance of the PIGMI Prototype", IEEE Trans. Nucl. Sci., NS-26 (3), 3767 (1979).
4. S.O. Schriber, E.A. Heighway and L.W. Funk, "Beam Tests with S-Band Standing Wave Accelerators Using On-Axis Couplers", Proc. of 1972 Proton Linac Conf., Los Alamos Scientific Laboratory Report LA-5115, 140 (1972).
5. M. Dazey, D. Nielsen, R. Robertson and D. Sewell, "RF Field Investigations on the 1/10 Scale Mark I Cavity", Radiation Laboratory Report UCRL-1173 (1951).
6. I.M. Kapchinskii and V.A. Teplyakov, "Linear Ion Accelerator with Spatially Homogeneous Strong Focusing", Prib. Tekh. Eksp., # 2, 19 (1970).
7. K.R. Crandall, R.H. Stokes and T.P. Wangler, "RF Quadrupole Beam Dynamics Design Studies", Proc. of 1979 Linac Conf., Brookhaven National Laboratory Report BNL-51134, 205 (1979).
8. J. Ungrin, J.C. Brown, B.G. Chidley, G.E. McMichael and S.O. Schriber, "Initial Operation of a 100% Duty Factor 3 MeV Alvarez Linac", proceedings of this conference.
9. S.O. Schriber, "Room-Temperature Cavities for High-Beta Accelerating Structures", Proc. of Conf. on Future Poss. for Electron Accel., Univ. of Virginia, L-1 (January 1979).
10. S.O. Schriber, "High-Beta Linac Structures", Proc. of 1979 Linac Conf., Brookhaven National Laboratory Report BNL-51134, 164 (1979).
11. J. McKeown, "Experience at Chalk River with a cw Electron Accelerator", Proc. of Conf. on Future Poss. for Electron Accel., Univ. of Virginia, K-1 (January 1979).
12. M.A. Allen and L.G. Karvonen, "High Duty Factor Structures for e^+e^- Storage Rings", Proc. of 1976 Proton Linac Conf., Atomic Energy of Canada Limited, Report AECL-5677, 175 (1976).
13. S.B. Hodge, L.W. Funk and S.O. Schriber, "Mechanical Design Considerations of a Standing Wave S-Band Accelerator with On-Axis Couplers", *ibid.*, 344 (1976).
14. J.M. Potter, LASL, private communication.
15. J. McKeown and S.O. Schriber, "Accelerating Structure with On-Axis Couplers for Electron Storage Rings", proceedings of this conference.